

This is the peer reviewed version of the following article:

Compressibility behavior and pressure-induced over-hydration of zeolite K- AlSi-L / Gigli, Lara; Vezzalini, Giovanna; Quartieri, Simona; Arletti, Rossella; Arletti, Rossella. - In: MICROPOROUS AND MESOPOROUS MATERIALS. - ISSN 1387-1811. - 276:(2019), pp. 160-166. [[10.1016/j.micromeso.2018.09.031](https://doi.org/10.1016/j.micromeso.2018.09.031)]

Terms of use:

The terms and conditions for the reuse of this version of the manuscript are specified in the publishing policy. For all terms of use and more information see the publisher's website.

05/01/2026 18:22



Compressibility behavior and pressure-induced over-hydration of zeolite K–AlSi-L

Lara Gigli^{a,*}, Giovanna Vezzalini^b, Simona Quartieri^c, Rossella Arletti^{d, e}

^a Elettra Sincrotrone Trieste, Basovizza, TS, Italy

^b Dipartimento di Scienze Chimiche e Geologiche, Università di Modena e Reggio Emilia, Via Giuseppe Campi 103, 41125, Modena, Italy

^c Dipartimento di Scienze Matematiche e Informatiche, Scienze Fisiche e Scienze della Terra, Università di Messina, Viale Ferdinando Stagno d'Alcontres 31, 98166, Messina S. Agata, Italy

^d Dipartimento di Scienze della Terra, Università di Torino, Via Valperga Caluso 35, 10125, Torino, Italy

^e Interdepartmental Centre "Nanostructure Interfaces and Surfaces NIS", Via Pietro Giuria 7, 10125, Torino, Italy

ARTICLE INFO

Keywords:

Zeolite L
High-pressure
XRPD
Structure refinement
Compressibility
Pressure induced hydration

ABSTRACT

This paper reports a study, performed by in-situ synchrotron X-ray powder diffraction, of the high-pressure behavior of zeolite L. The experiments were performed using both penetrating (methanol: ethanol: water mixture, m.e.w.) and non-penetrating (silicon oil, s.o.) pressure transmitting media (PTM) to study the compressibility and the possible pressure-induced hydration (PIH) of this synthetic zeolite, technologically relevant as host-guest system exploited in numerous application fields. The experiments were performed from P_{amb} to 6.2 and 6.3 GPa in s.o. and m.e.w., respectively. The crystal structure refinements were performed up to 6.3 GPa and 3.1 GPa for the patterns collected in m.e.w. and s.o., respectively, while the unit cell parameters were determined in the whole pressure range for both media. A strong PIH effect is evident when zeolite L is compressed in m.e.w. and the over-hydration is essentially ascribable to the filling of most the H_2O sites, to the appearance of a new H_2O site and to the partially filling of the K sites. The over-hydration starts at a very low pressure (0.5 GPa) and the maximum H_2O content can be estimated in 31.1 H_2O molecules, against the original value of 18. The PIH is completely reversible upon P release. The main difference between the compression behavior of zeolite L in the two media is the higher compressibility in the non-penetrating one, evidenced by $\Delta V = -6.3\%$ and -9.9% in m.e.w. and s.o., respectively. Our data are consistent with the general behavior of zeolites compressed with penetrating media, when the intrusion of H_2O molecules hinders the effects of the applied pressure. The results of this work are compared with those obtained on a K-gallosilicate with LTL topology, where PIH induces the formation of H_2O nanotubes inside the zeolite channel.

1. Introduction

The regular pore systems of the framework make zeolites ideal host matrices for achieving supramolecular organization of different molecules such as photo-active species, leading to versatile building blocks for the production of multifunctional composite materials [1,2]. Since the nanometric diameter channels of zeolites may induce an anisotropic arrangement of photoactive molecules, the resulting hybrid materials show outstanding energy transfer capabilities, mimicking the functionalities of the antenna systems of living plants [3–5] and can be exploited for several advanced applications [6–9]. The properties of these materials depend on the packing of molecules inside the channels, which in turn controls the intermolecular interactions. The packing of the molecules inside the channel can be modified by increasing

the molecules loading, or, for example, applying pressure. Notwithstanding, several studies have dealt with the incorporation of dyes into zeolites [10–15], only a work [16] until now exploited the behavior of these systems under high pressure trying to establish whether compression could favor a different distribution of the dye molecules and lead to an improvement of the optical properties of the materials under investigation. Very recently, Gigli et al. [16] studied the high-pressure behavior of some hybrid composites formed by zeolite L and fluorenone dye, through an integrated experimental-computational approach. The hybrid system resulted to be very stable upon pressure, undergoing only a modest variation of the pore volumes, thus affecting only to a minor extent the molecular structure of the organic guests. Only a pressure-induced strengthening of the interaction between the fluorenone carbonyl group and the potassium cations of the zeolite was observed. These results are clearly related to the stiffness of the host zeolite framework, thus unravel that the P-induced deformations of the

* Corresponding author.

Email address: lara.gigli@elettra.eu (L. Gigli)

pristine host framework is of fundamental importance to understand the driving forces involved in the hybrid structural modifications.

The appealing of zeolite L with LTL framework type [17] as host matrix for many applications is due to the narrow openings (free diameter 7.8 Å) and maximum diameter (~12 Å) of its mono-dimensional channel system. Since its first synthesis in 1968 [18], LTL framework has been associated to various cationic forms and hydration status [19–21] and has been found in the natural phase perialite [22]. In this study, the response to pressure of the as-synthesized K-LTL zeolite (K-L from now on) is discussed in details. The study was conducted by means of in-situ synchrotron X-ray powder diffraction (SR-XRPD) using both penetrating (methanol:ethanol:water = 16:3:1; m.e.w.) and non-penetrating (silicone oil; s.o.) pressure-transmitting media (PTM). We have studied stability, compressibility and pressure-induced over-hydration (PIH) of the as-synthesized phase K-L. Moreover, our results will be compared to those obtained by Lee and coworkers [23] on a K—GaSi-LTL phase compressed in m.e.w., with the aim to deepen our knowledge on the relationships between compressibility and framework/extraframework content of the porous materials.

2. Experimental

2.1. Material and crystal structure

The LTL framework is composed of cancrinite cages stacked via 6-ring windows to form columns of alternating hexagonal prisms and cancrinite cages along the *c*-axis. These columns are connected together to form a monodimensional channel system constituted by the larger circular 12-ring channels (12MR) and the smaller elliptical 8-ring channels (8MR), both running along the *c* axis. The extra-framework K cations are sited at the center of the cancrinite cage (K2), in the center of the elliptical 8-ring channel midway between adjacent cancrinite cages (K3), and near the walls of the main undulating 12-ring channel near the (001) plane at *z* = 0 (K4) (Fig. 1 and Tables S2 and S3). All the H₂O molecules are located in the main 12-ring channels near the planes at *z* = 0, 1/6, 1/3, and 1/2 and are only loosely bonded to the framework. The H₂O molecules on the latter three planes form clusters via hydrogen bonds, while those on the *z* = 0 plane coordinate the cations in the main channel.

Potassium zeolite L was purchased from Tosoh Corporation (Japan) (code HSZ-500). The chemical composition of the zeolite was determined by X-ray fluorescence and thermogravimetric analysis, resulting in the chemical formula $K_{8.46}(Al_{8.35}Si_{27.53})O_{72} \cdot 17.91H_2O$.

2.2. Methods

The in situ high-pressure XRPD experiments were performed at ALBA synchrotron, BL04-MSPD beamline, using a modified Merrill-Bas-

set DAC [24]. Two experiments were performed, using s.o. and m.e.w. as non-penetrating and penetrating PTM, respectively. The corresponding wavelengths were 0.534 and 0.5336 Å. Pressure was measured using the ruby fluorescence method [25] on the non-linear hydrostatic pressure scale [26]. The estimated error in the pressure values is 0.05 GPa. Bidimensional diffraction patterns were recorded on a CCD camera, SX165 (Rayonix) (pixel dimension 79 μm) at a fixed distance from the sample of 160 mm for the experiment in s.o. and 155 mm for that in m.e.w.; the exposure time was 50 s for all the pressure points. One-dimensional diffraction patterns were obtained in the 2θ range 1.5–27° by integrating the two-dimensional images with the program FIT 2D [27] (Fig. 3a and b). The experiments were performed from P_{amb} to 6.2 and 6.3 GPa in s.o. and m.e.w., respectively. Other patterns were recorded while decompressing the samples down to room conditions (labeled (rev) in Tables and Figures). The unit cell parameters of K-L were determined by Rietveld profile fitting in the complete *P* ranges (Table 1). Data quality allowed the K-L structure refinements up to 3.1 GPa and 6.3 GPa, in s.o. and m.e.w., respectively, and upon decompression to ambient conditions (P_{amb} (rev)). In the pressure range 3.09–6.2 GPa, the peak broadening induced by compression in s.o. allowed only the refinements of the cell parameters.

Since the analysis of the observed diffraction patterns did not show any phase transition, all the structural refinements were carried out in the original K-L space group *P6₃/mmm*, starting from the atomic coordinates reported by Gigli et al. [16] and using the GSAS package [28] with EXPGUI interface [29]. To allow the comparison with previous literature data on K-gallosilicate with LTL topology, the atom labels were after Lee et al. [23]. The background curves were fitted by a Chebyshev polynomial function with 32 and 24 coefficients in s.o. and m.e.w. experiments, respectively. The pseudo-Voigt profile function proposed by Thomson et al. [30] was used with refined Gaussian (GW) e Lorentzian (LX) terms and a 0.01% cut-off was applied for the peak intensities. The scale factor and 2θ-zero shift were accurately refined in all patterns. Soft constraints were imposed on the tetrahedral bond lengths (Si—O = 1.63 Å, with a tolerance value of 0.03 Å). The isotropic displacement parameters were allowed to vary and constrained in the following way: the same value for all the tetrahedral cations, a second group-value for the all framework oxygen atoms, a third one for the oxygen atoms of the H₂O molecules, while the isotropic displacement parameters of the potassium extraframework cations were not constrained to be equal. Details of the structural refinements are reported in Table S1. Atomic coordinates, site occupancies and isotropic displacement parameters are reported in Table S2 for m.e.w. experiment (2.5, 4.2, 6.3 GPa and P_{amb} (rev).) and in Table S3 for s.o. experiments (0.9, 1.2, 1.8, 3.1, 6.2 GPa and P_{amb} (rev)). Extraframework interatomic distances are listed in Tables S4 and S5 for m.e.w. and s.o. experiments respectively.

3. Results

From the inspection of Fig. 2, it is evident that the diffraction peak intensities generally decrease and the peak profiles become broader with increasing pressure. These effects can be ascribed to an increase of long-range structural disorder, the presence of texture effects, and, in the case of s.o. above 2.8 GPa, with a decrease in the hydrostaticity of the PTM [31]. However, both experiments demonstrate that K-L does not undergo amorphization up to the highest investigated pressure, and that the features characteristic of the patterns collected at ambient conditions are almost completely recovered upon decompression.

3.1. K-L compressed in methanol:ethanol:water

The compression of K-L in hydrous penetrating PTM from P_{amb} to 6.3 GPa reduces the unit cell volume by 6.2%, with a strongly

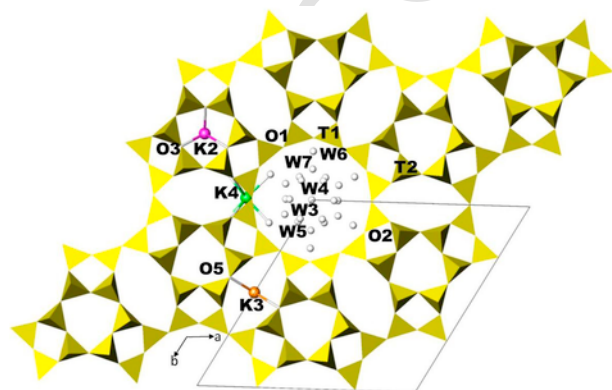


Fig. 1. K-L zeolite structure model view down [001].

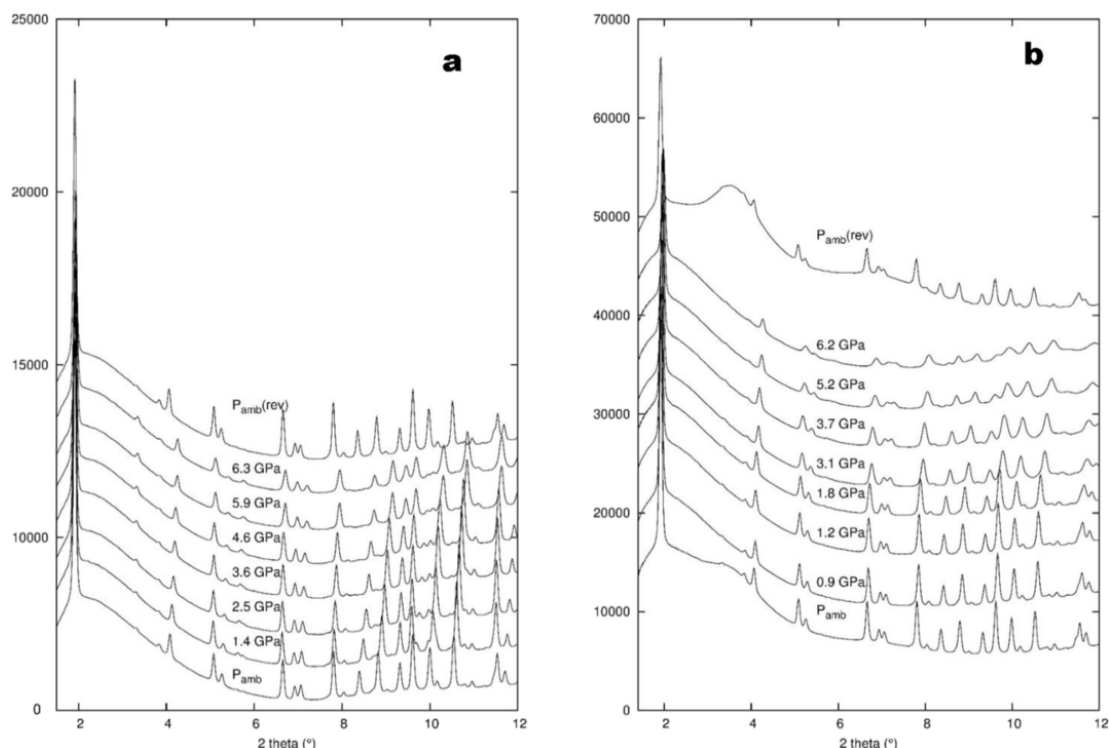


Fig. 2. Selected powder patterns for K-L compressed methanol:ethanol:water = 16:3:1 (m.e.w.) (a) and silicone oil (s.o.) (b) as a function of pressure.

anisotropic behavior of the cell parameters ($\Delta a = -0.8\%$, $\Delta c = -4.7\%$) (Table 1 and Fig. 3a). In particular, while the unit-cell edge along the c axis decreases almost regularly, the a axis slightly increases up to 2 GPa and then starts to decrease, resulting in a slight change in the volume compression above 2 GPa (Fig. 3a). At $P_{\text{amb}}(\text{rev})$, after complete pressure release, K-L unit cell volume almost regains the original value, maintaining a contraction of only 0.1%.

3.1.1. Extraframework cation sites

K2 and K3 sites remain fully occupied during the whole compression ramp. While K3 coordination does not change, that of K2 increases from 6 to 12 after the inclusion in its coordination shell of six O5 oxygen atoms, (Tables S2 and S4). The coordination of K4 site remains almost constant along the whole pressure ramp, while its occupancy factor tends to increase with increasing pressure. At P_{amb} , K4 is partially occupied, probably by both potassium and H_2O molecules. This is suggested by the number of K cations (9.7) resulting in this site from the structure refinement performed using the scattering curve of potassium, that is slightly higher than that found by the chemical analysis (8.46). At 2.0 GPa the occupancy factor of K4 site begins to increase and at $P_{\text{amb}}(\text{rev})$ it almost regains the initial value.

A new site, labeled K5, appears at 1.4 GPa. Like K3, it is located at the center of the 8MR, but at $z = 0$, where coordinates four O6. Its occupancy increases with P up to a maximum value of about 0.50 at 6.3 GPa, then it disappears upon P release (Tables S2 and S4). Similarly to that suggested for K—GaSi-LTL compressed in m.e.w [23], we can assume that a fraction of K cations migrates from K4 to K5 and that, successively, both sites increase their occupancy factor hosting, in addition to K, also H_2O molecules, provided by the hydrous PTM. In this case, the coordination distances are compatible with those of H_2O molecules (Table S4).

3.1.2. H_2O sites

At ambient conditions, about 18 H_2O molecules per unit cell occupy the 12MR channels of K-L, – distributed over five crystallographically

independent sites (W3, W4, W5, W6, W7). Compression induces noticeable changes in both positions and occupancy factors of these H_2O sites. Concerning the occupancy factors, a general increase occurs for all the sites, with the only exception of W5, that tends to decrease above 3 GPa (Fig. 4 and S1). Upon pressure release, almost all the H_2O sites regain their original occupancy, with the exclusion of W4 and W6.

In detail, the behavior of the H_2O sites upon compression can be described as follows:

- A new site, labeled W2 hereafter following [23], appears at 0.5 GPa, with an occupancy factor of 0.16, at the special position (0, 0, 0.5) at the center of the main 12MR channel in correspondence of the 12MR window. Its occupancy factor increases up to 0.8 (Figure S1 and Table S2). Upon P release, W2 sites completely empties;
- W3 site moves, along b axis, closer to the 12MR channel walls and maintains this position even upon pressure release (Table S2). Its occupancy factor increases with P , even if with a rather irregular trend;
- W4 site, originally at the position (0, 0, 0.18), moves to the mirror plane at $z = 0$ and, up to the highest P , maintains this position. Upon P release, it almost reassumes the original position. In the H_2O clusters present at P_{amb} , W4 represents the apex of a bipyramidal-hexagonal prisms and its P -induced migration transforms the cluster in hexagonal prisms (Fig. 5). W4 occupancy factor increases already at 0.5 GPa and at 1.4 GPa the site becomes fully occupied;
- W5 site moves close to the mirror plane at $z = 0.5$ during compression. As a consequence of its shift, the distances with O1 largely change. Its occupancy factor decreases above 3 GPa (Figure S1 and Table S2). At $P_{\text{amb}}(\text{rev})$, W5 almost regains its original position;
- W6 site undergoes a slight positional change during compression, but at $P_{\text{amb}}(\text{rev})$ returns to the original position. The site becomes fully occupied at 0.5 GPa (Figure S1, and Table S2);
- W7 slightly changes its position, with a consequent decrease of its distance from O2. Its occupancy factor strongly increases, reaching the maximum of 0.8 at 3.6 GPa (Figure S1, and Table S2).

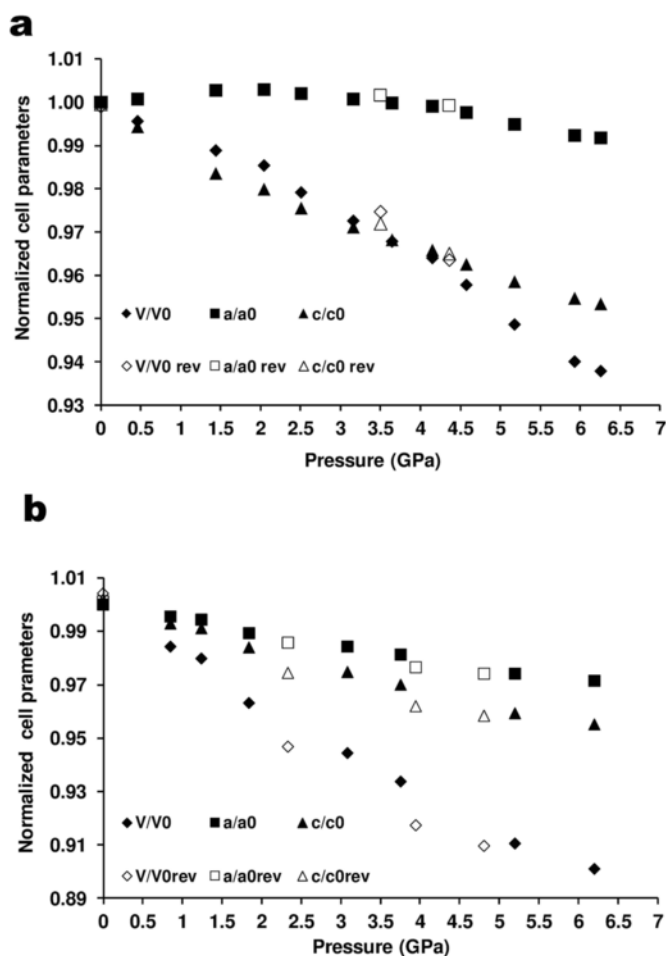


Fig. 3. Normalized unit cell parameters for K-L compressed in m.e.w. (a) and s.o. (b) as a function of pressure.

On the basis of these observations we can state that:

- a strong PIH effect is evident in zeolite K-L, as in many zeolites compressed with a penetrating PTM [32–35]. This effect is essentially ascribable to the filling of most of the H₂O sites, to the partially filling of K4 and K5 sites and to the appearance of the new H₂O site W2;
- over-hydration begins at a very low pressure (0.5 GPa) and reaches its maximum degree at 4.6 GPa; then it slightly decreases up to the highest investigated pressure (Fig. 4);
- the maximum H₂O content can be estimated in 31.1 molecules, assuming both the increased H₂O content of the W sites and that due to the residual electronic density in both K4 and K5, after subtraction of the contribution of the K cations;
- PIH is completely reversible upon *P* release.

The effects of PIH are evident on the unit cell volume behavior. Its decrease is slower below 2 GPa – namely during the over-hydration, when the H₂O molecules contribute to stiffen the framework – and faster above this pressure, when the external compression prevails.

3.1.3. Framework

The following modifications of the K-L framework are observed upon compression:

Table 1

Cell parameters of K-L compressed in m.e.w. and in silicone oil. * data relative to P_{amb} sample are taken from Ref. [14].

m.e.w			
Pressure (GPa)	<i>a</i> (Å)	<i>c</i> (Å)	<i>V</i> (Å ³)
P_{amb}^*	18.379(1)	7.528(1)	2202.4(1)
0.5	18.391(1)	7.485(1)	2192.8(1)
1.4	18.429(1)	7.403(1)	2177.8(1)
2	18.431(1)	7.376(1)	2170.3(1)
2.5	18.415(1)	7.343(2)	2156.6(1)
3.6	18.376(1)	7.288(1)	2131.5(1)
4.2	18.362(1)	7.269(1)	2122.9(1)
4.6	18.333(1)	7.245(1)	2109.2(1)
5.2	18.285(1)	7.215(1)	2089.3(1)
5.9	18.237(1)	7.186(1)	2070.2(1)
6.3	18.229(1)	7.176(1)	2065.3(1)
4.4 (rev)	18.364(1)	7.264(1)	2121.9(1)
3.5 (rev)	18.406(1)	7.316(1)	2146.8(1)
P_{amb} (rev)	18.375(1)	7.524(1)	2200.3(1)
s.o.			
Pressure (GPa)	<i>a</i> (Å)	<i>c</i> (Å)	<i>V</i> (Å ³)
P_{amb}^*	18.379(1)	7.528(1)	2202.4(1)
0.9	18.298(1)	7.474(1)	2167.6(1)
1.2	18.274(1)	7.461(1)	2158.0(1)
1.8	18.182(1)	7.408(1)	2121.0(1)
3.1	18.091(1)	7.338(1)	2080.1(1)
3.7	18.033(1)	7.302(1)	2056.7(1)
5.2	17.906(1)	7.221(1)	2005.1(1)
6.2	17.853(1)	7.189(1)	1984.6(1)
4.8 (rev)	17.905(1)	7.215(1)	2003.3(1)
3.9 (rev)	17.950(1)	7.241(1)	2020.7(1)
2.3 (rev)	18.117(1)	7.335(1)	2085.2(1)
P_{amb} (rev)	18.401(1)	7.542(1)	2211.7(1)

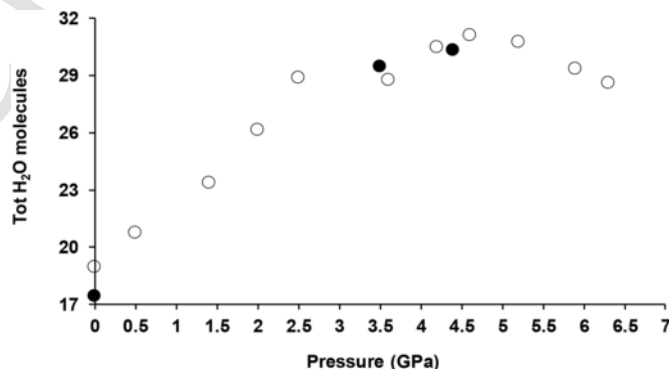


Fig. 4. Total number of H₂O molecules in K-L compressed in m.e.w. as a function of pressure. The full black symbols are associated to decompression ramp.

- The 12MR becomes more elliptical after the H₂O penetration, due to the slight decrease of O1—O1 free diameters (Figure S2a). At the highest pressure it almost regains the original shape;
- 8MR channel aperture expands up to 4.2 GPa with the increase of both O1—O1 and O5—O5 free diameters. Above this pressure, probably after reaching its largest acceptable size, 8MR aperture becomes more elliptical, with the O1—O1 distance decreasing and the O5—O5 slightly increasing (Figure S2b);
- the dimensions of the 8MR boat-shaped apertures surrounding the main 12MR channel undergo opposite modifications: O1—O1, corresponding to the *c* axis, regularly decreases in the whole *P* range, probably as a consequence of the strengthening of the W7—O2 interaction, while O6—O6 increases up to 2.5 GPa, decrease up to 4.5 GPa and then increases again, reaching the maximum value at the highest *P* (Figure S2c);
- O3—O5—O3 and O5—O3—O5 angles of the D6R hexagonal ring (Figure S2d) increase and decrease, respectively, becoming more

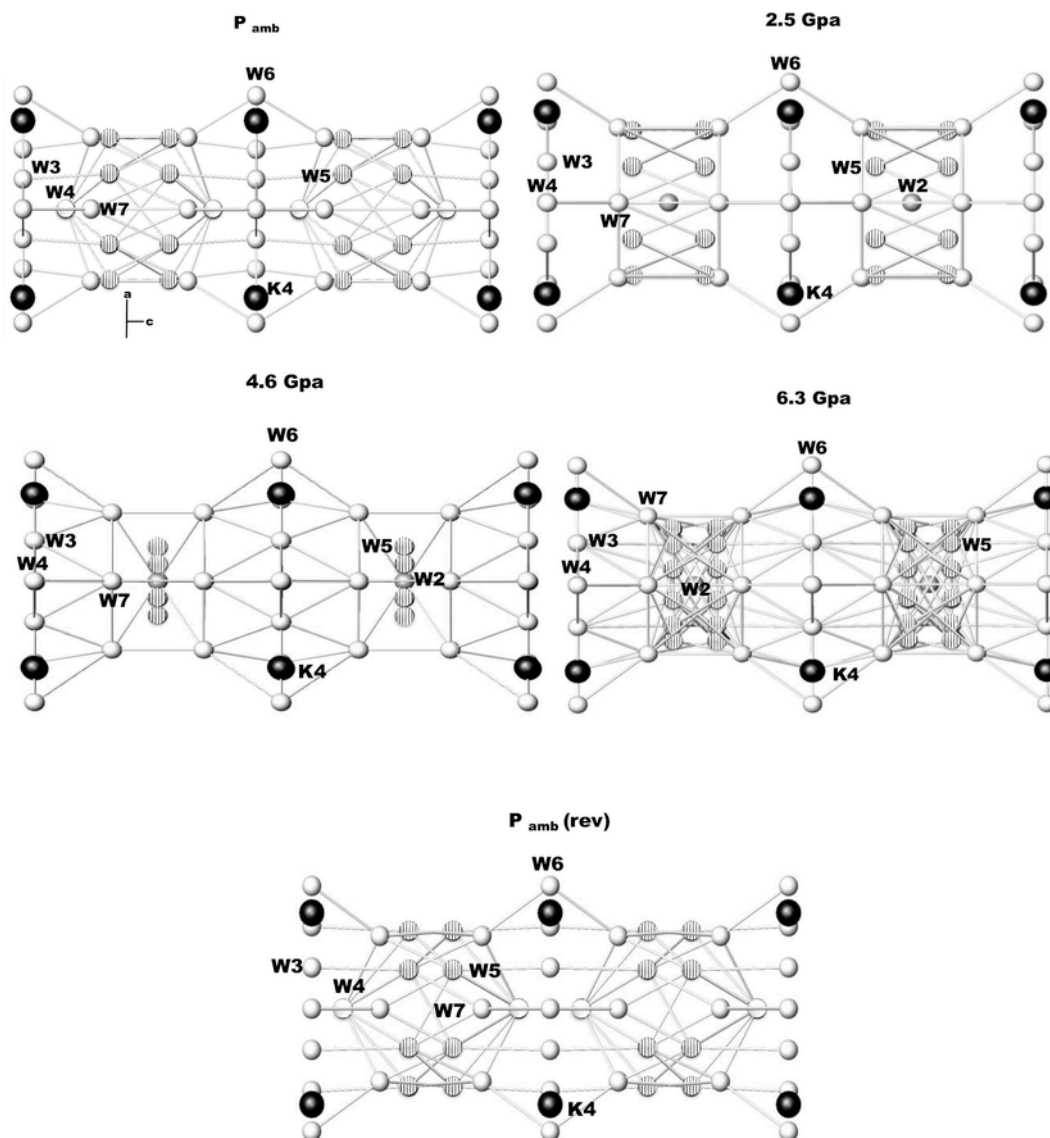


Fig. 5. H₂O molecules distribution (“nanotubes”) in K-L compressed in m.e.w. at selected pressure values. Black spheres = K atoms, grey spheres = W2 H₂O molecules, white spheres = all the other H₂O molecules. The possible hydrogen bonds among oxygen atoms of H₂O molecules are shown in the range 2.6–3.2 Å.

similar to each other, and hence reducing the di-trigonal distortion of the 6-membered ring. The D6R thickness only slightly changes (Figure S2e), initially increasing and then decreasing above 3.6 GPa. On the contrary, due the onset of the K2 — O5 bond, the thickness of the cancrinite cage decreases in the whole P range (Figure S2f), with a strict relationship with the c parameter.

In general, K-L framework appears much more flexible along the c axis - the running direction of the large 12MR channels - than along a axis. This can be an effect of the presence, on the ab plane, of both D6R building units and cancrinite cage columns, that contribute to stiffen the structure.

3.2. K-L compressed in silicone oil

The unit cell volume of K-L compressed from P_{amb} to 6.2 GPa in the non-penetrating PTM s.o. decreases by 9.9%, with a less anisotropic compressional pattern ($\Delta a = -2.9\%$, $\Delta c = -4.5\%$) with respect to the experiment in m.e.w. (Table S1 and Fig. 3b). Both cell parameters

show an almost linear contraction and at $P_{\text{amb}}(\text{rev})$, after pressure release, K-L unit cell volume almost regains the original value.

The main structural modifications observed during compression are:

- in the range P_{amb} –3.1 GPa - where the structural refinements were performed - both positions and occupancy factors of most of the H₂O sites remain essentially unchanged. Only W4 site moves significantly along the z axis (from about 0.20 to about 0.30), maintaining the new position also upon decompression (Table S3);
- the effects of compression in s.o. on the extraframework cations are similar to those observed in m.e.w.: K5 site appears at 1.8 GPa, with a very low occupancy factor, while the occupancy of K4 decreases. This behavior is even more evident at 3.1 GPa. Upon pressure release, K5 disappears (Table S3);
- concerning the framework, both the main 12MR and the 8MR channels parallel to the c axis contract, due to the decrease of their free diameters O1—O1 and O2—O2, and O1—O1 and O5—O5, respectively (Figure S3a,b);
- the 8MR apertures - nearly parallel to the c axis and surrounding the main 12MR channel - contract upon compression (Figure S3c);

- O3—O5—O3 and O5—O3—O5 angles of the D6R hexagonal ring (Figure S3d) decrease and increase, respectively. Consequently, the di-trigonal distortion of the 6-membered ring increases. The D6R thickness (Figure S3e) decreases with pressure, partially maintaining this flattening upon decompression;
- the cancrinite cage thickness regularly decreases with P , but, after pressure release, assumes a value larger than the original one (Figure S3f). As an effect of the combined decrease and increase of the D6R and cancrinite cage thickness, respectively, at $P_{\text{amb}}(\text{rev})$ the c unit cell parameter regains the original value.

4. Discussion

The overall results here reported underline the high baric stability of LTL framework and confirm the results found by Ref. [16] for zeolite L-fluorenone hybrid material. In particular, the compressibility in s.o. of the as-synthesized K-L is similar to that determined for a K-L loaded with 0.5 fluorenone molecules (see Fig. 6). This suggests that the stiffening effect of the dye molecule - associated to the presence of H_2O molecules (14.7) and K cations - is comparable to that of the extraframework content of the pristine sample. However, the small variations of the elastic behavior observed among the LTL samples characterized by different dye loadings, suggest that an influence of the extraframework content is detectable.

4.1. Comparison between the compressibility of zeolite K-L in penetrating and non-penetrating PTM

The main difference between the behavior of K-L compressed in m.e.w. and s.o. is the higher compressibility in the non-penetrating PTM (see Fig. 2a and b and Table S1). This is evident by the comparison of the unit cell volume decrease induced by the two PTM at the highest pressure: 6.3% in m.e.w. against -9.9% in s.o. In particular, while c parameter contracts of the same value in both experiments, a parameter decreases more in s.o., due to the squeezing of both 12MR and 8MR windows. On the contrary, in m.e.w., the contraction of the 12MR aperture and the expansion of the 8MR one tend to balance each other. Moreover, the ditrigonal distortion of the D6R increases with P in s.o., while decreases in m.e.w., thus contributing to the larger squeezing in the a - b plane. The decrease of c parameter with s.o. is related to the flattening of both cancrinite cage and D6R f, while in m.e.w. the effect on the cancrinite cage prevails.

These results are consistent with the behavior generally observed for zeolites undergoing intrusion phenomena: the penetration of extra-

molecules stiffen the structure, providing a support against the effects of compression (e.g. for a review, see Table 1 in Ref. [36]).

4.2. Comparison between the behavior of K—AlSi-L and K—GaSi-L zeolites compressed in m.e.w

Lee and coworkers [23] have discussed how H_2O molecules penetrate and evolve into a K—GaSi-L (chemical formula $\text{K}_{12.1}\text{Ga}_{10.3}\text{Si}_{25.7}\text{O}_{72} \cdot \sim 16\text{H}_2\text{O}$) when compressed to 3.37 GPa in m.e.w.

The evolution of K—GaSi-L unit cell parameters with P is similar to that of the aluminosilicate phase here investigated, except for the maximum value of the unit cell edge along the a axis, that is reached at a lower pressure (1.3 GPa) in K—GaSi-L with respect to K-L (2.0 GPa). This difference affects the pressure at which the curve V vs. P changes slope in the two samples (1.3 GPa in the K—GaSi-L and 2.0 GPa in K-L, Fig. 3b of this work and Fig. 2b in Ref. [23]). Moreover, in K—GaSi-L the variation of a parameter in the range P_{amb} -1.3 GPa is 0.38%, while that of K-L in the range P_{amb} -2.0 GPa is only 0.28%. However, when a similar P range is considered (P_{amb} -3.5 GPa), the unit cell parameter variations are essentially the same in the two phases ($\Delta a = +0.003\%$, $\Delta c = -3.24\%$, $\Delta V = -3.23\%$ and $\Delta a = -0.02\%$, $\Delta c = -3.29\%$, $\Delta V = -3.22\%$ for the gallo- and the aluminosilicate, respectively). This suggests that the framework/extra-framework composition of this zeolite is not a dominant factor in influencing its compressibility, at least at relatively low pressure and in penetrating PTM.

In K—GaSi-L, the variations of the occupancy factors of K4 and K5 sites with pressure are strictly inversely related, suggesting a P -induced migration of K cations from K4 to K5. At 3.5 GPa, however, this new K5 site returns empty. On the contrary, in our K-L sample, K5 is occupied up to the highest pressure and the penetration of H_2O molecules in both K4 and K5 sites is progressive and continuous during compression.

At ambient conditions, K—GaSi-L contains 16 H_2O molecules, assembled inside the undulating 12-ring channels into hydrogen-bonded clusters alternated with H_2O layers (note that in Ref. [23] the possible hydrogen bonds are accepted in the range 2.55–2.9 Å). With increasing PIH, the interactions among the H_2O molecules increase and both H_2O clusters and H_2O layers are interconnected to form hydrogen-bonded H_2O nanotubes inside the zeolite channels. The nanotubes close the 12MR channel access, hindering a further H_2O penetration, and gradually transform into isolated species, interacting only with the zeolite framework. The evolution of these H_2O nanostructures is linked to associated framework distortions and cation migration, which appear to be driven by the gradual “flattening” of the host 12-ring channels.

At ambient conditions, the H_2O content of the aluminosilicate here studied is higher (18 H_2O molecules) and an additional H_2O site W7 - not found in the K—GaSi-L - is present. If a larger, and more meaningful, hydrogen bonding distance range of 2.6–3.2 Å is assumed, the H_2O nanotube structure is already present in K-L at P_{amb} (Fig. 5). Actually, at this pressure only W6—W7 bond is always present, due to the very high occupancy factor of W6 site. Otherwise, due to the low occupancy factors of the other H_2O sites, all the other H_2O — H_2O bonds must be considered only statistically present. Above 2.5 GPa, as a consequence of the PIH, W4 and W6 sites are completely filled, the occupancy factors of W2 and W3 are near 0.8 and that of W7 becomes 0.8 at 3.6 GPa. With increasing pressure, and the consequent shifts of W4 and W5, the H_2O — H_2O interactions change, but the nanotube structure is maintained up to the highest pressure.

During compression, the nanotube modifications are driven by the shifts of W5 and W4 sites and by the strengthening of the interactions of W5 and W7 with the framework oxygen atoms O1 and O2, respectively. Hence, the hypothesis proposed by Lee and co-workers [23] that pressure contributes to the dissociation of the H_2O nanostructures in K

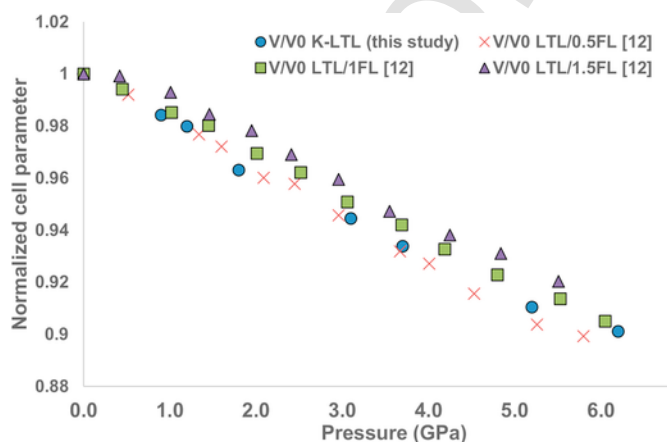


Fig. 6. Comparison among the pressure dependent volume variations of pristine zeolite K-L and hybrid K-L samples loaded with different amount of fluorenone (PTM silicone oil).

—GaSi-L, cannot be applied to K—AlSi-L phase. In fact, our results, covering an even larger P range, demonstrate that the H₂O nanotubes are statistically present from ambient to the highest investigated pressure of 6.3 GPa.

Acknowledgments

This work was supported by the Italian MIUR, within the frame of the following projects: PRIN2015 “ZAPPING” High-pressure nano-confinement in Zeolites: the Mineral Science know-how APPLIED to engineering of innovative materials for technological and environmental applications” (2015HK93L7). ALBA Synchrotron Light Facility is acknowledged for allocating beam time at the beamline BL04 – MSPD.

Appendix A. Supplementary data

Supplementary data to this article can be found online at <https://doi.org/10.1016/j.micromeso.2018.09.031>.

References

- [1] G. Calzaferri, *Langmuir* 28 (2012) 6216–6231.
- [2] G. Calzaferri, R. Méallet-Renault, D. Brühwiler, R. Pansu, I. Dolamic, T. Dienel, P. Adler, H. Li, A. Kunzmann, *ChemPhysChem* 12 (2011) 580–594.
- [3] V. Martínez-Martínez, R. García, L. Gómez-Hortigüela, R. Sola Llano, J. Pérez-Pariente, I. López-Arbeloa, *ACS Photonics* 1 (2014) 205–211.
- [4] P. Li, Y. Wang, H. Li, G. Calzaferri, *Angew. Chem. Int. Ed.* 53 (2014) 2904–2909.
- [5] A. Devaux, G. Calzaferri, I. Miletto, P. Cao, P. Belser, D. Brühwiler, O. Khorev, R. Häner, A. Kunzmann, *J. Phys. Chem. C* 117 (2013) 23034–23047.
- [6] M.M. Tsotsalas, K. Kopka, G. Luppi, S. Wagner, M.P. Law, M. Schafers, L. De Cola, *ACS Nano* 4 (2010) 342–348.
- [7] Z. Li, G. Luppi, A. Geiger, H.-P. Josel, L. De Cola, *Small* 7 (2011) 3193–3201.
- [8] A. Szarpak-Jankowska, C. Burgess, L. De Cola, J. Huskens, *Chem. Eur. J.* 44 (2013) 14925–14930.
- [9] H. Manzano, L. Gartzia-Rivero, J. Bañuelos, I. López-Arbeloa, *J. Phys. Chem. C* 117 (2013) 13331–13336.
- [10] A. Devaux, G. Calzaferri, P. Belser, P. Cao, D. Brühwiler, A. Kunzmann, *Chem. Mater.* 26 (2014) 6878–6885.
- [11] L. Gartzia-Rivero, J. Bañuelos, I. López-Arbeloa, *Materials* 10 (2017) 495.
- [12] V. Martínez-Martínez, R. García, L. Gómez-Hortigüela, R. Sola Llano, J. Pérez-Pariente, I. López-Arbeloa, *ACS Photonics* 1 (2014) 205–211.
- [13] R. Sola-Llano, Y. Fujita, L. Gómez-Hortigüela, A. Alfayate, H. Ujii, E. Fron, S. Toyouchi, J. Perez-Pariente, I. Lopez-Arbeloa, V. Martinez-Martinez, *ACS Photonics* 5 (2017) 151–157.
- [14] L. Gigli, R. Arletti, G. Tabacchi, E. Fois, J.G. Vitillo, G. Martra, G. Agostini, S. Quartieri, G. Vezzadini, *J. Phys. Chem. C* 118 (2014) 15732–15743.
- [15] L. Gigli, R. Arletti, J. Vitillo, G. Alberto, G. Martra, A. Devaux, G. Vezzadini, *J. Phys. Chem. C* 119 (2015) 16156–16165.
- [16] L. Gigli, R. Arletti, E. Fois, G. Tabacchi, S. Quartieri, V. Dmitriev, G. Vezzadini, *Crystals* 8 (2018) 79–101.
- [17] C. Baerlocher, L.B. McCusker, D.H. Olson, *Atlas of Zeolite Framework Types*, sixth ed., Elsevier, Amsterdam, 2007.
- [18] D.W. Breck, N.A. Acara, U.S. Patent 711 (1968) 565.
- [19] R.M. Barrer, H.Z. Villiger, *Kristallogr* 128 (1969) 352–370.
- [20] Ch Baerlocher, R.M. Barrer, *Z. Kristallogr.* 136 (1972) 245–254.
- [21] J.M. Newsam, *Mater. Res. Bull.* 21 (1986) 661–672.
- [22] G. Artioli, Å. Kvik, *Eur. J. Mineral* 2 (1990) 749–759.
- [23] Y. Lee, C.-C. Kao, S.J. Kim, H.-H. Lee, D.R. Lee, T.J. Shin, J.-Y. Choi, *Chem. Mater.* 19 (2007) 6252–6257.
- [24] R. Miletich, D.R. Allan, W.F. Kush, *Rev. Mineral. Geochem.* 41 (2000) 445–519.
- [25] R.A. Forman, G.J. Piermarini, J.D. Barnett, S. Block, *Science* 176 (1972) 4673–4676.
- [26] H.K. Mao, J. Xu, P.M. Bell, *J. Geophys. Res.* 9 (1986), 4673–4676.
- [27] A.P. Hammersley, S.O. Svensson, M. Hanfland, A.N. Fitch, D. Häusermann, *High Pres. Res.* 14 (1996) 235–248.
- [28] A.C. Larson, R.B. Von Dreele, *General Structure Analysis System “GSAS”*, vols. 86–748, Los Alamos National Laboratory Report LAUR, 1994.
- [29] B.H. Toby, *J. Appl. Crystallogr.* 34 (2001) 210–213.
- [30] P. Thomson, D.E. Cox, J.B. Hastings, *J. Appl. Cryst.* 20 (1987) 79–83.
- [31] R.J. Angel, M. Bujak, J. Zhao, G.D. Gatta, S.D. Jacobsen, *J. Appl. Cryst.* 40 (2007), 26–3.
- [32] G. Vezzadini, R. Arletti, S. Quartieri, *Acta Crystallogr. B* 70 (2014) 444–451.
- [33] P. Lotti, R. Arletti, G.D. Gatta, S. Quartieri, G. Vezzadini, M. Merlini, V. Dmitriev, M. Hanfland, *Microporous Mesoporous Mater.* 218 (2015) 42–54.
- [34] R. Arletti, C. Giacobbe, S. Quartieri, G. Vezzadini, *Minerals* 7 (2017) 18–33.
- [35] R. Arletti, E. Fois, L. Gigli, G. Vezzadini, S. Quartieri, G. Tabacchi, *Angew. Chem. Int. Ed.* 56 (2017) 2105–2109.
- [36] S. Ori, S. Quartieri, G. Vezzadini, V. Dmitriev, *Am. Mineral.* 93 (2008) 1393–1403.